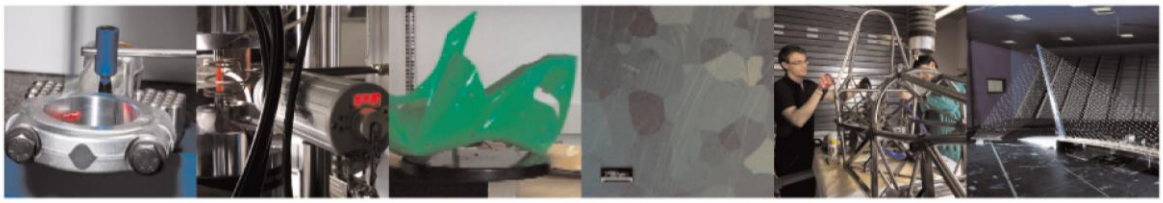

Dross-free submerged laser cutting of AZ31 Mg alloy for biodegradable stents

Demir, Ali Gökhan; Previtali, Barbara

DIPARTIMENTO DI MECCANICA ■ POLITECNICO DI MILANO
via G. La Masa, 1 ■ 20156 Milano ■ EMAIL (PEC): pecmecc@cert.polimi.it
http://www.mecc.polimi.it
Rev. 0

Dross-free submerged laser cutting of AZ31 Mg alloy for biodegradable stents

Ali Gökhan Demir*, aligokhan.demir@polimi.it

Barbara Previtali, barbara.previtali@polimi.it

Department of Mechanical Engineering, Politecnico di Milano, Via La Masa 1, 20156 Milan, Italy

*Corresponding author

Dross-free submerged laser cutting of AZ31 Mg alloy for biodegradable stents

Ali Gökhan Demir*, aligokhan.demir@polimi.it

Barbara Previtali, barbara.previtali@polimi.it

Department of Mechanical Engineering, Politecnico di Milano, Via La Masa 1, 20156 Milan, Italy

*Corresponding author

Abstract

Submerged cutting of AZ31 Mg alloy was studied with ns-pulsed green fiber laser and three different submersion liquids namely, water, alcohol-water solution and paraffin based oil. Compared to conventional laser cutting with coaxial process gas, differences due to optical, chemical and mechanical effects were identified. An analytical solution was introduced to assess the fluence decay due to beam enlargement and absorption in the submersion liquid. The chemical reactions between the Mg alloy and submersion liquid were defined and weight loss due to chemical effects was studied in static immersion tests. The mechanical instability related to liquid breakdown was studied to reveal the threshold levels for the liquids. The interaction of these mechanisms was studied within process. The results showed dross-free cutting is achievable by submerging the Mg alloy in 0.5 mm alcohol-water solution, which shows a processing condition that enables chemical dissolution of dross without excessive fluence loss or liquid instability. The cut quality of the optimized conditions was comparable to fs-pulsed laser cutting of the same material.

Keywords: Laser microcutting; Submerged cutting; Biodegradable stents; Mg alloys; Green fiber laser

1. Introduction

Stent manufacturing conventionally uses laser microcutting on tubular precursors to incise the stent mesh [1-3]. The laser microcutting operation is often followed by chemical and electrochemical polishing steps to improve the surface quality of the implant. One of the surface defects generated during laser microcutting is the dross

formation, when lasers operating with ms to ns pulses are used [4]. Around the cut kerf molten material resolidifies generating the dross layer. Laser sources with ps to fs pulse durations avoid heat generation inside the material, hence reduce dross formation. Elimination or reduction of the consecutive surface cleaning processes in stent manufacturing are of industrial interest both for permanent and biodegradable materials. The chemical etching and electrochemical polishing processes are difficult to control and add up to the production costs and complexity. Biodegradable Mg alloys constitute further problems in cleaning surface finishing operations due to high corrosion rate. Previous work showed that the dross type and quantity are essential factors for ease of cleaning of Mg alloy stents [5]. Excessive dross generation with CW laser results in prolonged exposure to chemical attack, hence considerable reduction in the stent thickness. Femtosecond pulsed laser microcutting generates powder residue on surface, which is cleaned easily with a moderate chemical etching step and the underlying surface quality is very good.

Another approach to reduce or eliminate the dross problem is by submerged laser processing [6,7]. The common submersion liquid is water which contributes by reducing the dross and heat affected zone on laser processing. Applied as a surface film, water was shown to improve material ablation while processing with UV, VIS and IR laser sources [8]. Laser ablation of aluminum with a 800 nm wavelength Ti:sapphire laser under 1 mm of water increased etch rate drastically [9]. The use of water submersion for laser micromachining of Si was also demonstrated to reduce recast and redeposited layers [10]. More recently, the use of alcohol-based submersion liquids in laser microdrilling has been demonstrated, showing reduced surface damage and improved hole geometry compared to dry processing [11,12]. Acidic solutions as submersion liquid have also been proposed, which realize a chemically assisted laser microcutting process on chemically stable metals such as stainless steel [13]. Concerning stent manufacturing, use of assistance liquid has been demonstrated both on and below the cut surface. In a conventional laser stent cutting system consisting of a conventional cutting head with coaxial gas flow, wet cutting can be achieved by flowing water in the cut tube. The results showed reduced backwall damage and heat affected zone on stainless steel due to effective cooling provided by water [14]. On the other hand, submersion cutting of nitinol in 1 mm thick water showed better surface finish and absence of recast with a fs laser [15].

The use of green wavelength in laser micromachining operations has been studied in literature making use of different laser sources, such as pulsed copper vapor lasers (λ=510-580 nm) [16], Nd:YAG lasers in second harmonic wavelength (λ=532 nm) [17-19] and more recently Yb:fibre lasers with second harmonic generation [20]. These works showed higher etch rate on highly reflective materials and improved machining quality compared to 1 μm wavelength. Another appealing aspect of the green wavelength is its transmittance in water. Hence, water jet guided laser systems often use Nd:YAG lasers with second harmonic generation [21]. These use of the water jet enables maintaining small beam size along the jet length, hence machining structures with high aspect ratio becomes possible. The quality is also improved by reduced dross generation. Water jet guided laser cutting is also applied with continuous wave Yb:fibre and Nd:YAG lasers operating at 1 μm wavelength, despite the lower transmittance of water around this wavelength due to higher laser powers available [22,23].

It can be seen that the majority part of the literature deals with the final quality achieved by liquid assisted laser processes. As a matter of fact, the whole system consisting of laser, liquid and workpiece material gives way to infinite combinations for how the liquid assisted laser process can be employed. The main effects contributing to the enhanced processing in the presence of the assisting liquid can be decomposed and studied. This way, the process design can be facilitated. This work describes the submerged cutting of AZ31 Mg alloy for biodegradable stent manufacturing from this point of view. Three different submersion liquids with different optical and physical properties were employed to improve the cut quality. A pulsed green fiber laser operating with 1 ns pulse duration was employed for high transmittance in water. The optical changes were analyzed by analytical modelling, chemical effects were studied through static corrosion tests in the submersion liquids, and liquid breakdown under laser irradiance was studied for mechanical effects. The interaction of these effects was investigated in process, through morphological analysis of the realized samples. The results showed dross-free cutting in alcohol-water solution and as well as providing indications to designing new liquids for submerged cutting.

2. Materials and submerged laser cutting system

Cold rolled 0.25 mm-thick sheets of AZ31 Mg alloy (3 wt% Al, 1 wt% Zn, bal. Mg) were used throughout the experiments (Goodfellow Cambridge, Huntingdon, England). Three different submersion liquids were tested

namely pure water (Bessone Srl, Mondovì, Italy), a commercially available ethanol-water solution (90 vol. % ethanol, 2 vol. % methyl-ethyl-ketone, Sai Spa, Modena, Italy), lubricant oil (65 vol. % heavy paraffin hydrocarbon, 27 vol. % naphthenic hydrocarbon, 8 vol. % aromatic hydrocarbon and 0.3 vol. % S, Singer, Indaiatuba, Brasil). For the sake of simplicity, the cutting liquids will be referred hereafter as water, alcohol and oil.

Table 1. Optical and physical properties of the submersion liquids and cut material

	n	**k**	**α [cm^{-1}]**	**R_{al}**	**R_{ls}**	**T_B [K]**	**ρ [g/cm^3]**	**K [W/mK]**	**η [mPa·s]**
Water	1.3335	0.124e-6	0.029	2.0%	47%	373	0.99	0.598	1.002
Alcohol	1.3640	1.768e-6	0.418	23.7%	46.4%	351	0.79	0.167	1.074
Oil	1.4642	0.074e-6	0.018	3.6%	44.1%	433	0.90	0.150	9.6
AZ31	2.8735	3.359	8e5			1363	1.77	96	

Table 2. The main specifications of IPG Photonics YLPG-5 laser.

Wavelength	λ	532 nm
Pulse duration	τ	1 ns
Max. average power	P_{avg}	6 W
Max. pulse energy	E_p	20 µJ
Pulse repetition rate	PRR	20-300 kHz
Beam quality factor	M^2	1.12
Collimated beam diameter	d_c	3.5 mm
Focal length	f	100 mm

The optical properties of the cutting liquids have been characterized by a double beam spectrophotometer (V570 from Jasco). Using the transmission data at 532 nm wavelength, the complex refractive index of the liquids were calculated. For the refractive index of AZ31 reference data for opaque metals was used [24]. The reflectivity calculated with the reference data corresponded well to the measured reflectivity at 532 nm wavelength in air with

the same spectrophotometer (R_{as}=56%). Material optical properties, as well as boiling point (T_B), density, thermal conductivity (K) and viscosity (η) are summarized in Table 1.

A pulsed fiber laser operating at second harmonic was employed as the light source (YLPG-5 from IPG Photonics, Oxford, MA, USA). The laser source is based on master oscillator power amplifier (MOPA) architecture and emitted at 532 nm wavelength and 1.2 ns pulse duration. The laser pulse repetition rate (PRR) range is 20-300 kHz with maximum pulse energy at 20 µJ. The measured average and estimated peak power are 6 W and 16 kW respectively. The output beam was 3.29 mm in diameter with M^2=1.2. The beam was focused using 100 mm focal lens (AC254-100-A-ML from Thorlabs, Newton, NJ, USA). The main specifications of the laser source are shown in Table 2. Workpiece positioning was achieved by linear stages (ACS-150 from Aerotech, Inc., Pittsburgh, PA, USA). The workpiece was submerged in different liquids in a PMMA container fixed on the moving stages, where the workpiece was positioned in a stainless steel fixture.

3. Modelling of predominant effects in submerged laser cutting

The presence of submersion liquid as a barrier between the workpiece and ambient atmosphere generates several differences compared to conventional laser cutting. Three main effects related to optical, chemical and mechanical phenomena, are described in general and investigated for the particular laser, submersion liquids and workpiece material combinations.

3.1. Optical effects

Compared to conventional laser cutting, in submerged cutting the laser beam passes through a second transparent medium, which is the cutting liquid. During such passage the beam divergence changes. The addition of the liquid barrier generates interfaces for reflection between air and liquid and between liquid and solid workpiece. The propagation of beam in submerged cutting is schematized in Figure 1. The portion of the light transmitted through the cutting liquid will be also attenuated as a function of liquid column height. In the end, the combination of these effects change the fluence reaching the workpiece as expressed in:

$$F_0 = \frac{8E_T}{\pi d_s^2} \quad (1)$$

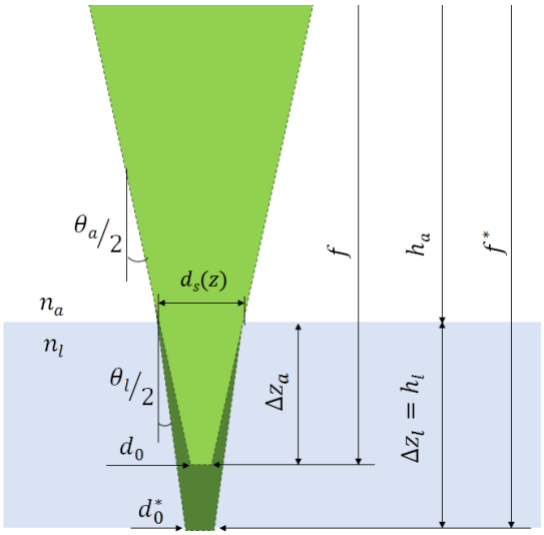

Figure 1. Schematic representation of beam propagation in submersion liquid.

where E_T is the transmitted energy arriving on the workpiece and d_s is the laser spot diameter on the workpiece. Both transmitted energy and spot radius depend on the liquid height. The transmitted energy on the workpiece can be calculated considering the reflections at the interfaces and attenuation according to Beer-Lambert law from the following expression:

$$E_T = (1 - R_{al})Ee^{-\alpha h_l}(1 - R_{ls}) \quad (2)$$

where E is the incident laser energy, R_{al} and R_{ls} are the reflectivity at air-liquid and liquid-solid interfaces respectively, α is the absorption coefficient and h_l is the height of the liquid column. Reflectivity and absorptivity properties of a material are linked to the complex refractive index:

$$\tilde{n} = n + ik \quad (3)$$

where n is the real part of the refractive index and k is the imaginary part called extinction coefficient. The absorption coefficient is thus calculated using extinction coefficient for a given wavelength (λ) using the following relationship:

$$\alpha = \frac{4\pi k}{\lambda} \quad (4)$$

On the other hand, the reflectivity at the interface of two media can be calculated using The Fresnel's equation:

$$R_{ij} = \left|\frac{\widetilde{n_i}-\widetilde{n_j}}{\widetilde{n_i}+\widetilde{n_j}}\right|^2 \quad (5)$$

where the subscripts refer to the complex refractive index belonging to different media. On the other hand, the change in divergence should be considered in order to calculate the beam radius on the workpiece. Beam divergence in air (θ_a) after focal lens can be estimated as:

$$\theta_a = \frac{d_c}{f} \quad (6)$$

And the beam diameter at focal plane is calculated with the following equation:

$$d_0 = \frac{4\,M^2\,\lambda\,f}{\pi\,d_c} \quad (7)$$

where M^2 is the beam quality factor, λ is the wavelength, f is the focal length and d_c is the collimated beam diameter. According with Snell's law, when light passes from a with lower refractive index to another with higher refractive index, the refraction angle is smaller than the incidence angle. For the specific case of laser beam passing from air into the submersion liquid, the beam divergence changes, which also varies the geometrical position of the focal point. Therefore the modified focal length f^* is greater than the initial f. The Snell's law can be written:

$$n_a \sin\frac{\theta_a}{2} = n_l \sin\frac{\theta_l}{2} \quad (8)$$

where θ_l is the refraction angle in liquid. Rewriting Eq.8, refraction angle in liquid can be calculated as:

$$\theta_l = 2 \cdot \sin^{-1}\left(\frac{n_a}{n_l}\sin\frac{\theta_a}{2}\right) \quad (9)$$

where n_a and n_l are the refractive index of air and liquid respectively. As the refraction angle θ_l is smaller than the divergence angle of the laser beam in air θ_a, the geometrical focus position moves farther away from the focusing lens. Therefore to calculate the new position of minimum spot diameter in liquid condition d_0^*, the modified focal

length f^* due to the change of the geometrical focus position needs to be defined. As shown in Figure 1, the modified focal length depends on the distance between the focal lens and the surface of the liquid, h_a. The beam will focus in a new point at h_l distance from the liquid surface as the modified focal length will be at:

$$f^* = h_a + h_l \tag{10}$$

In a cutting process, the main requirement is to position the focal plane at a certain distance from the liquid surface. Hence h_l is a process parameter, whereas h_a is required be calculated. The caustic equation allows calculating spot size at a given Δz distance from the focal point, and can be expressed as:

$$d_s^2(z) = d_0^2 + \Delta z^2\, \theta^2 \tag{11}$$

According to Figure 1, the optical path can be divided into two main parts as the portion of the beam that propagates in air and the portion that propagates in the liquid. The beam size on the liquid surface can be used as a reference point where:

$$d_s^2(z) = d_0^2 + {\Delta z_a}^2\, \theta_a^2 = {d_0^*}^2 + {\Delta z_l}^2\, \theta_l^2 \tag{12}$$

where Δz_a is the distance between liquid surface and virtual position of d_0 and is equal to $f\text{-}h_a$, with $\Delta z_l = h_l$. In this equation the spot diameter in the liquid d_{0^*} can be calculated with the modified focal length f^* as:

$$d_0^* = \frac{4\, M^2\, \lambda\, f^*}{\pi\, d_c} = \frac{4\, M^2\, \lambda\, (h_a + h_l)}{\pi\, d_c} \tag{13}$$

Eq. 12 can be rewritten to substituting the unknown terms with their definitions to take the following form:

$$(Cf)^2 + (f - h_a)^2 \theta_a^2 - \big(C(h_a - h_l)\big)^2 - h_l^2 \theta_l^2 = 0 \tag{14}$$

where C is a constant and is expressed as:

$$C = \frac{4\, M^2 \lambda}{\pi d_c} \tag{15}$$

Eq. 14 can be solved to obtain h_a as a function of h_l. The second order form will produce two solutions for h_a, however only one solution represents the physical reality where $h_a<f$. Once h_a is calculated, the modified focal length f^* and the diameter of the laser beam in this position d_0^* can be calculated using Eq.10 and Eq.13. Figure 2 shows the calculated f^* and d_0^* values in different cutting liquids as a function of liquid height h_l, and using the complex refractive indexes reported in Table 1. Figure 2 shows the calculated values as a function of liquid height for the considered submersion liquids. It can be noted that for the green laser wavelength the geometrical focal position changes between 2 and 3 mm for liquid height of 10 mm. The corresponding increase in spot diameter is lower than 1 µm. The biggest enlargement of laser spot is observed for oil, due to its higher refractive index.

Assuming that during the cutting operation, the geometrical focal position inside the cutting liquid is positioned on the material surface (i.e. the material surface is placed at f* distance from the focusing lens), the Eq.2 can be rewritten to calculate fluence as a function of h_l:

$$F_{0,l} = \frac{8E_T}{\pi(d_0(h_l))^2} = \frac{8}{\pi d_0^{*2}}(1-R_{al})E_I e^{-\alpha h_l}(1-R_{ls}) \tag{16}$$

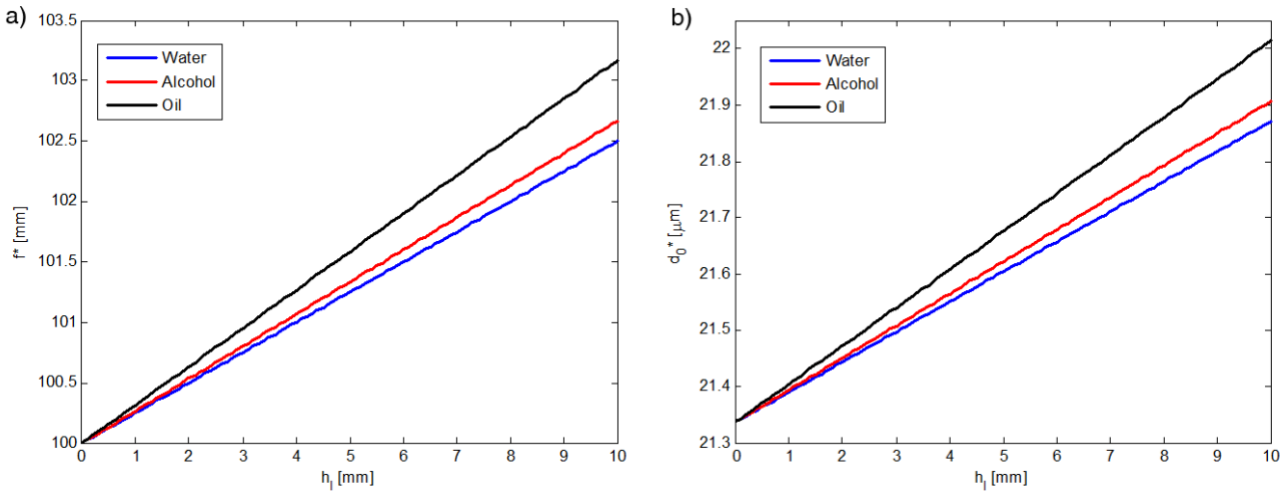

Figure 2. Modified focal length (f^*) and the spot size (d_0^*) on the virtual focal point as a function of liquid height (h_l) calculated for the different submersion liquids.

Substituting the energy term in Eq. 1 and Eq. 2 with pulse peak power (P_p), Eq. 16 can be also written for irradiance (I_0). Figure 3.a shows the transmittance expressed as the proportion of transmitted energy to incident energy on the liquid surface as a function of liquid height. It can be seen that a large fraction of energy is lost due to reflections

at air-liquid and liquid-solid interfaces. The difference in reflectance between the liquids can be comprehended between the offsets of the curves. The difference between the decay rates are due to the absorption coefficients of the liquids. It can be seen that oil and water maintain almost constant transmittance as a function of liquid height. Due to low reflectance at the interfaces the maximum overall loss in oil ($1-E_{T,min}/E=48\%$) is lower than the reflectance in air ($R_{as}=56\%$). Similar observation for alcohol can be made with a slightly higher the maximum overall loss compared to oil ($1-E_{T,min}/E=51\%$). This indicates that the submersion liquid may enhance the absorbed amount of laser energy by the workpiece. Alcohol on the other hand shows a pronounced decay due to the higher absorption coefficient. Above 3 mm of alcohol, the energy loss exceeds the amount of energy lost in air. At 10 mm of alcohol, 75% of laser energy is lost to reflection and absorption in liquid. In Figure 3.b. the proportion of fluence on workpiece in submersion liquid to fluence in air is shown. The plot incorporates the influence of beam enlargement due to change in refractive index with transmission data. It can be seen that the influence of beam enlargement is reduced compared to losses in transmission. On the same plot, the ordinate on right hand side represents the calculated fluence absorbed by the workpiece. The maximum fluence in air using the available system is 11.4 J/cm^2. Depending on the liquid type and height the absorbed fluence varies between 3.7 and 6.2 J/cm^2.

The present model represents stable submersion conditions. Stable conditions refer to liquid with constant height and without disturbances. The movement of positioning system can cause fluctuations resulting in non-homogenous height distribution as well as changes in surface normal. Another factor is related to the instabilities generated by gaseous phase in the submersion liquid. If the liquid absorbs too much energy directly from the laser beam or the heated workpiece, this may generate bubbles. The expansion of the ablation plasma and plume are other sources of instability.

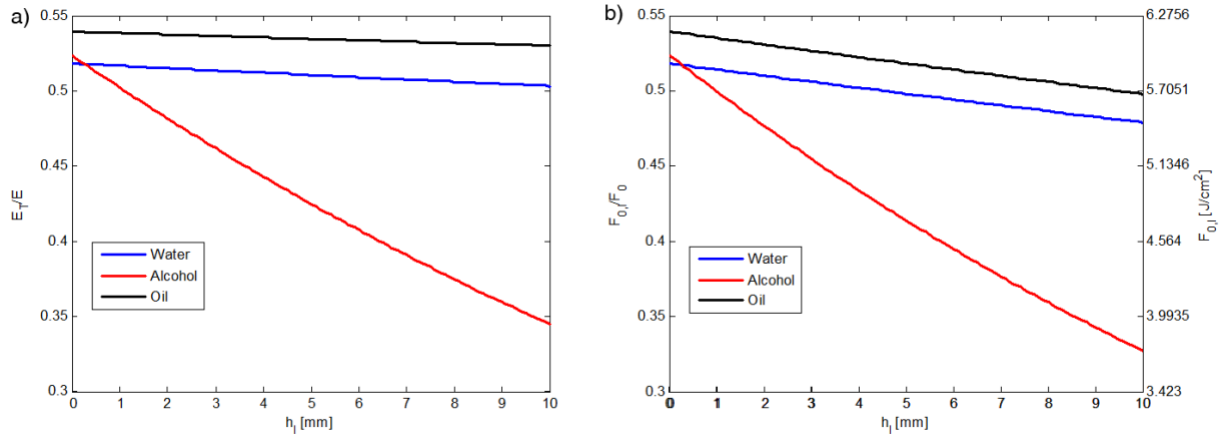

Figure 3. a) Transmittance, b) proportion of fluence in liquid to fluence in air and corresponding fluence levels as a function of liquid height (h_l) calculated for the different submersion liquids.

3.2. Chemical effects

Compared to other metals, chemical effects are more pronounced for Mg and its alloys due to their high reactivity. The in-process corrosion caused by the submersion liquid can be of aid to the cutting operation, if it contributes to material removal. Accordingly the possible chemical reactions and the reaction products should be considered in view of material removal. Magnesium oxidizes easily in ambient atmosphere due to its high affinity to oxygen and generates MgO according to:

$$Mg + \frac{1}{2}O_2 \rightarrow MgO \tag{17}$$

In air at normal ambient temperature, magnesium has a good oxidation resistance, due to the generated protective MgO film. On the contrary, the wet environment degrades this film and forms less stable hydrated oxide. In dry air but at high temperature (above 723 K), magnesium oxide begins to decompose and consequently it is not protective anymore. In particular during the degradation of the protective film, the oxidation rate is constant and visibly appears as a porous and white surface layer [25]. From laser processing view point, the generated MgO layer is much more difficult to cut due to the higher melting temperature compared to Mg [4].

In aqueous environments, magnesium is dissolved electrochemically to form magnesium hydroxide and hydrogen according to following reaction:

$$Mg + 2H_2O \rightarrow Mg(OH)_2 + H_2 \quad (18)$$

This hydroxide film has hexagonal structure that facilitates its separation from the metal. The film formed in water on Mg alloys, is sensitive to temperature, agitation and contaminants. In fact, the corrosion rate in water may increase by one or two orders of magnitude when the temperature rises above 373 K.

In environments that contain ethanol, magnesium is transformed into magnesium ethoxide and hydrogen according to the following reaction:

$$Mg + 2C_2H_6O \rightarrow C_4H_{10}MgO_2 + H_2 \quad (19)$$

Magnesium ethoxide decomposes at relatively low temperature (543 K), which is expected to facilitate the cutting procedure [26]. Regarding oil, no chemical reaction is expected to occur, because it consists mainly of paraffin hydrocarbons.

In order to test the effect of submersion liquid on the corrosion behaviour of the AZ31 alloy static immersion tests were employed. The tests were conducted in a way to gather main insights to the differences in chemical etching rate of the different liquids. Under the laser cutting conditions, the chemical reactions are expected to be accelerated, mainly due to high temperature at the cut kerf vicinity. Test specimens with 20x50 mm^2 dimensions were cut and weighted prior to submersion in the liquids. Five different samples were immersed in 50 mL liquid in different containers. The samples were maintained at room temperature and weighted in 2-3 days intervals to monitor the weight change for a total duration of 24 days. The specimens after the immersion tests were visually investigated. The specimens submerged in water and alcohol showed darkened colour with white oxide marks on the surface. Moreover, they showed surface topography change due to localized and pitting corrosion. The specimens submerged in oil did not show any significant change on the surface regarding colour or roughness. Figure 4 shows the weight change as a proportion of the measured weight to the initial weight (w/w_0). The weight loss in water appears below 1% over the duration of the test. Alcohol generates up to 2% weight loss, depicting a more aggressive environment for the Mg alloy. The variability of weight loss in alcohol also appears lower, as depicted by the lower standard deviation values compared to other liquids (see Figure 4). The reduced variability

between replications of the same condition points to a more stable material removal, which is definitely advantageous for the submerged laser cutting application. While a linear behaviour in the weight decrease is observed in water, an asymptotic behaviour is present in alcohol. Submersion in oil results in increase of weight. Since a chemical reaction is not present between the Mg alloy and oil, the increase is due to entrapment on the surface. Hence, the submersion cutting applied in oil requires a washing procedure to remove the oil residue on the surface.

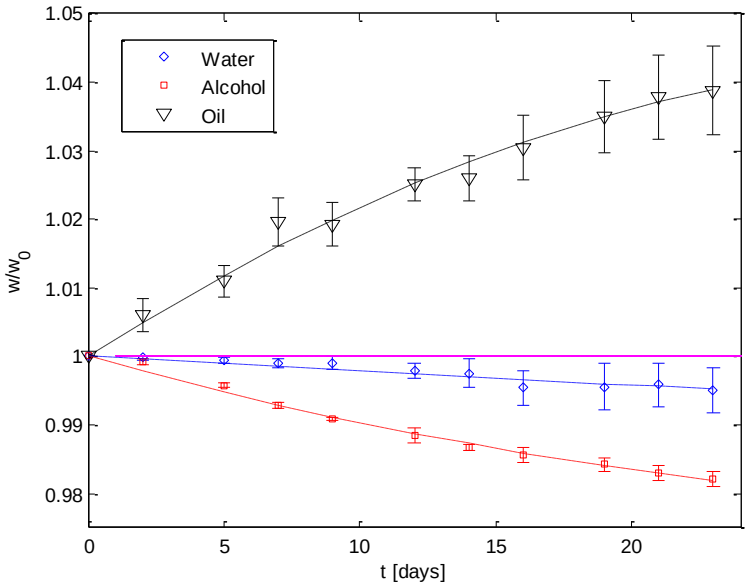

Figure 4. Weight change of AZ31 specimens in different submersion liquids as a function of time.

3.3. Mechanical effects

During submerged cutting, the mechanical effects are mainly related to plasma expansion. Plasma can generate both from the metallic workpiece and submersion liquid. Kennedy et al [27] reported that the laser pulse, focused into a volume of aqueous fluid, will cause breakdown when the irradiance in the focal volume surpasses the breakdown threshold. This breakdown produces a dense plasma that increases its temperature (6000 to 15000 K) and pressure (20 to 60 kbar) by inverse Bremsstrahlung absorption, when the laser pulse remains in the focal volume after plasma formation. The plasma absorbs visible radiation much more than transparent matter and can

block the transmission of the light due to the phenomenon of plasma shielding. When the plasma tends to expand along the laser beam, phenomenon called moving breakdown, produces cylindrical cavitation in liquids. During this phenomenon the plasma shielding cools the plasma and limits its expansion. Another phenomenon produced by plasma absorption is the acoustic shockwave due to the expansion of the plasma at supersonic velocities. After the end of laser pulse, the plasma cools and implodes. This last process occurs through energy losses for three causes: shock wave emission, optical emission and thermal conduction into the surrounding liquid. The kerf obtained in submerged cutting can be larger than in dry condition due to two primary reasons: i) high-density shock wave due to the liquid confinement effect that deflects the beam; ii) mechanical erosion due to plasma implosion and generation of vapour bubbles, that introduce a significant impact force towards the workpiece.

Accordingly, the stability of the liquid under laser irradiation was tested by launching the beam directly inside the liquid without the workpiece. The liquid tank was filled with 20 mm liquid and the beam focus was positioned at 10 mm liquid height, by compensating the focal position as expressed in Eq.10. Throughout the experiments, the beam was kept stationary. The laser energy and pulse repetition rate were varied between 0.5-20 µJ and 50-300 kHz respectively. The liquid instability was observed qualitatively in the form of cylindrical cavitation around the beam path, matching the conditions of moving breakdown. The minimum energy condition resulting in liquid instability was registered as the critical condition. Table 2 reports the observed critical conditions for the used submersion liquids. Liquid instability occurred in water with the highest level of energy, whereas liquid instability was observed in alcohol and oil in relatively low energy levels due to higher absorption coefficients. As reported in Table 2, the corresponding peak power levels are between 1-10 kW, which result in high peak power intensity or irradiance (I) at the focal point. The fluence ($F_{0,c}$) and irradiance ($I_{0,c}$) levels at the critical conditions can be calculated using Eq.16, where R_{ml} is equal to zero. Accordingly, the irradiance at the focal point reaches up to 5.03 GW/cm$_2$, which the liquid cannot withstand. It can be concluded that alcohol and oil are more likely to deviate the laser beam generate mechanical erosion during cutting compared to water. These effects can be beneficial for material removal or disadvantageous since the irradiance reaching the material is reduced.

Table 3. The critical conditions generating liquid instability.

Liquid	f* [mm]	d_0* [µm]	E [µJ]	Pp [kW]	PRR [kHz]	$F_{0,c}$ [J/cm^2]	$I_{0,c}$ [GW/cm^2]
Water	102.5	21.9	11.93	9.9 kW	300	6.35	5.03
Alcohol	102.7	21.9	1.66	1.4 kW	50	0.88	0.47
Oil	103.2	22.0	1.66	1.4 kW	50	0.87	0.69

4. Experimental study of submerged laser cutting quality of AZ31

The laser cutting quality in submersion liquids was investigated as a function of cutting speed (v), submersion liquid type and height (h_l) and compared to dry cutting. Four levels of cutting speeds between 0.25 and 5.25 mm/s were selected. The levels of liquid height, 0.5 and 4 mm were used. In all experiments the focal position was placed on material surface, by adjusting the focal distance according to the calculated f* values. The laser energy and pulse repetition rates were set to the highest values, 20 µJ and 300 kHz respectively. Two linear incisions, 10 mm in length, were realized and each combination was replicated twice. The workpiece material was immersed in a liquid tank, which had 80 x 80 mm^2 surface area. The relatively large surface area provided a uniform submersion liquid distribution with low liquid heights, by avoiding meniscus formation. Moreover, the liquid height was set in the middle of the sample, where the cutting experiments were made to avoid capillary effects around the liquid tank borders. In order to assess the cutting quality, dross area (A_{dross}) at the top surface was measured. SEM images taken from top. The total dross area on both sides of the kerf over 740 µm of incision length was measured, as schematized in Figure 5. The measurement variability was evaluated from repeated measurements over the same image, and the calculated standard deviation was 910 µm^2. Cross sections were realized, which were then used to measure top and bottom kerf width (w_{top} and w_{bottom}). Taper was calculated using the kerf width measurements according to:

$$\phi = \tan^{-1}\left(\frac{w_{top}-w_{bottom}}{2t}\right) \quad (20)$$

where t is the material thickness.

Table 4. Experimental plan for the study of submerged laser cutting quality

Fixed parameters		
Focal position	Δz [mm]	0

Pulse energy	E [μJ]	20
Pulse repetition rate	PRR [kHz]	300

Varied parameters		
Cutting liquids		Dry, water, alcohol, oil
Liquid level	h_l [mm]	0.5, 4.0
Cutting speed	v [mms/s]	0.25, 1.50, 2.75, 4.00, 5.25

Measurements		
Dross area	A_{dross} [μm2]	
Top kerf width	w_{top} [μm]	
Bottom kerf width	w_{bottom} [μm]	
Taper	ϕ [o]	

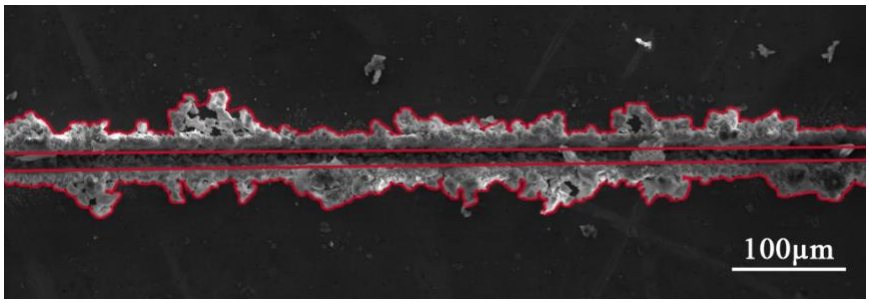

Figure 5. Example of dross area measurement procedure.

4.1. Analysis of experimental study and discussion

Through Figure 6 to Figure 10 the cut kerf morphologies obtained with different parameter combinations are depicted. The experimental study showed that complete cuts were not achievable with h_l=4 mm. Figure 6 depicts the top side of the cut kerfs obtained in different cutting liquids with 0.25 mm/s cutting speed. The dry cuts show deposited dross around and inside the cut kerf. The experimented conditions in the water showed intermittent cuts without any dross and very large kerfs. With alcohol, large and irregular kerfs could be achieved. On the other hand, the laser generated only a trace on the AZ31 sheet when submerged in oil. As shown in Figure 7, the increase of cutting speed, reduces cut depth under water and alcohol, whereas in oil the trace of laser path becomes less evident. At 5.25 mm/s cutting speed, there is no sign of material removal under alcohol and oil, while under water a similar morphology is present with decreased kerf depth. The 4 mm liquid height is expected to absorb too much laser energy and eventually to cause breakdown during the cutting operation in all cases.

Through cuts could be achieved with 0.5 mm liquid height in most of the experimented conditions. Figure 8 reports the SEM micrographs of the cuts realized with 0.25 mm/s cutting speed. Significant improvement in cut quality is visible with alcohol and oil, whereas submersion in water does not produce through cuts also in this case. The top and bottom sides of cuts realized with alcohol are dross free with very limited amount of powderous residue around the kerf. Submersion in oil produces dross only inside the kerf. Increasing the cutting speed, dross amount as well as morphology increases for dry, alcohol and oil conditions (see Figure 9 and Figure 10). In dry cutting, the dross morphology consists of micrometric particles with flake shape for all cutting speeds. Under alcohol the morphology changes from micrometric flake shaped debris to powderous residue, around 2.75 mm/s cutting speed. The change in morphology implies that the chemical attack of alcohol starts taking effect only above a certain energy density. By lowering the cutting speed, pulse overlap increases, which results in higher energy density. The same dross morphology is obtained under 4 mm liquid height with the same cutting speed, which strengthens the hypothesis. The dross morphology of oil is similar to that of dry cutting and does not change with cutting velocity. Overall, for all cutting conditions, the bottom side of the kerf is irregular starting from 2.75 mm/s cutting speed. Once regular kerf is achieved below 2.75 mm/s alcohol provides a clean kerf both inside the kerf and on the bottom side. Despite providing a clean kerf bottom below 2.75 mm/s cutting speed, oil produces dross accumulation inside the kerf. In the absence of chemical effects, oil provides only mechanical means to evacuate the dross from the opened kerf. However, due to high viscosity oil cannot run through the opened kerf, which is expected to result in accumulating some of the dross inside the kerf.

Overall, in water the material removal appears to be accompanied by mechanical erosion and chemical attack. The enlarged kerf is caused by the instable beam and erosion generated by the collapse of bubbles. In alcohol, ablation is expected to be accompanied by chemical removal. The higher volatility of alcohol reduces the effect of mechanical erosion. Submersion in oil blocks the laser radiation to effectively reach the workpiece material. Due to chemical stability, material removal is not accompanied by the chemical reaction. The high viscosity (η) of the liquid is expected to generate a damping effect on the collapse of the bubbles.

Figure 11 depicts the cross sections of the cuts realized in 0.5 mm liquid height and 0.25 mm/s cutting speed. Straight walls are achieved in dry conditions and with submersion in alcohol. The cross section of cut obtained in oil is less regular compared to the previous two. Submersion in water on the other hand results in a V-shaped trench, characterized by a larger opening on the top side. The discovered geometry strengthens the hypothesized machining condition based on chemical attack and mechanical erosion. It is expected that the generated plasma restricts the laser beam to reach deeper in the machined material, but the mechanical erosion enlarges the kerf width.

The measurements related to kerf quality and geometry are reported in Figure 12. It can be seen that starting from 4 mm/s of cutting speed there is no remarkable material removal in water as the top kerf width is zero (Figure 12.a). Overall, the top kerf width remains very similar for dry, alcohol and oil conditions, as the values decay from 40 µm to 20 µm as a function of cutting speed. On the bottom side of the kerf (Figure 12.b), measured widths are very similar for dry condition and alcohol (w_{bottom}=10-12 µm). The lower kerf width obtained in oil with the lowest cutting speed can be attributed to the high viscosity of the liquid preventing the generated dross to move out and deposit inside the kerf as observed in Figure 8. The resulting taper values are restricted between 2° and 3° for the through cuts achieved with dry, oil and alcohol conditions between 0.25 and 2.75 mm/s (Figure 12.c). The dross area increases with an asymptotic rise as a function of cutting speed. In oil and alcohol there is a clear overall decrease compared to dry cutting. Dross-free cuts could be achieved starting from 1.5 mm/s for oil and at 0.25 mm/s for alcohol. No dross was observed for cut conditions in water, depicting no advantage for improved quality since the cuts were not through. A regression model was fitted explain the trend in dross reduction as a function of process parameters. For this purpose only the stable conditions, namely, dry, alcohol and oil with 0.5 mm liquid height were considered, where the cutting condition is a categorical variable. It was found out that the dross reduction trends were statistically the same for alcohol and oil. Hence, the categorical variable "condition" consisted of two groups, dry and submerged (alcohol and oil). The final fitted model consisted of two equation, where the constant term varies for different cutting conditions. For dry cutting,

$$A_{dross}[\mu m^2] = 18638 + 9544 \cdot v[mm/s] - 1009 \cdot (v[mm/s])^2 \quad (21)$$

whereas for alcohol and oil,

$$A_{dross}[\mu m^2] = 9544 \cdot v[mm/s] - 1009 * (v[mm/s])^2 \quad (22)$$

The model fits the data well as illustrated in Figure 12.d, and as indicated by the high R_{2adj} value at 96.6%. The model shows that the effect of cutting speed is the same in all conditions, and statistically confirms that the use of oil and alcohol effectively minimises the dross amount.

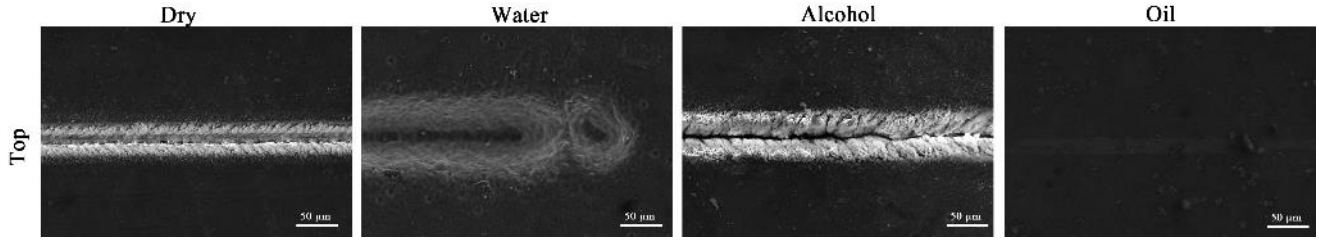

Figure 6. Comparison of dry cutting and submerged cutting conditions with 4 mm liquid height and 0.25 mm cutting speed.

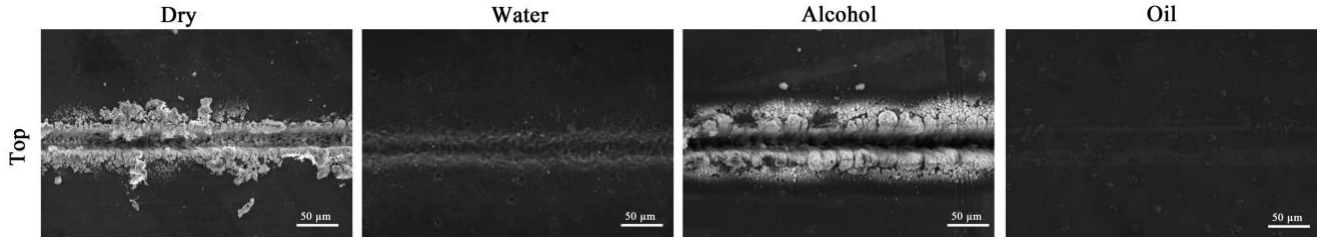

Figure 7. Comparison of dry cutting and submerged cutting conditions with 4 mm liquid height and 2.75 mm cutting speed.

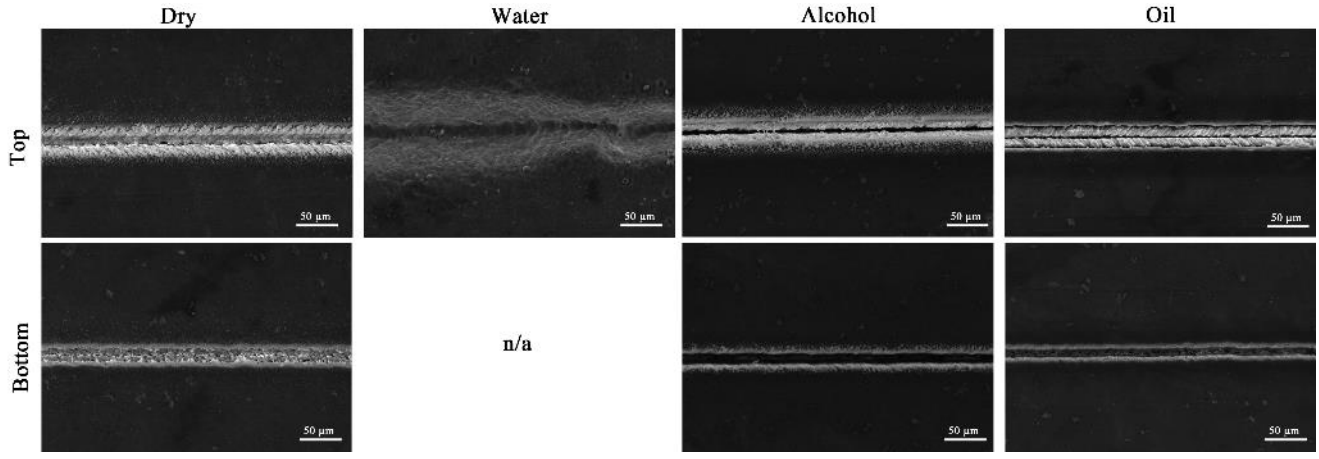

Figure 8. Comparison of dry cutting and submerged cutting conditions with 0.5 mm liquid height and 0.25 mm cutting speed.

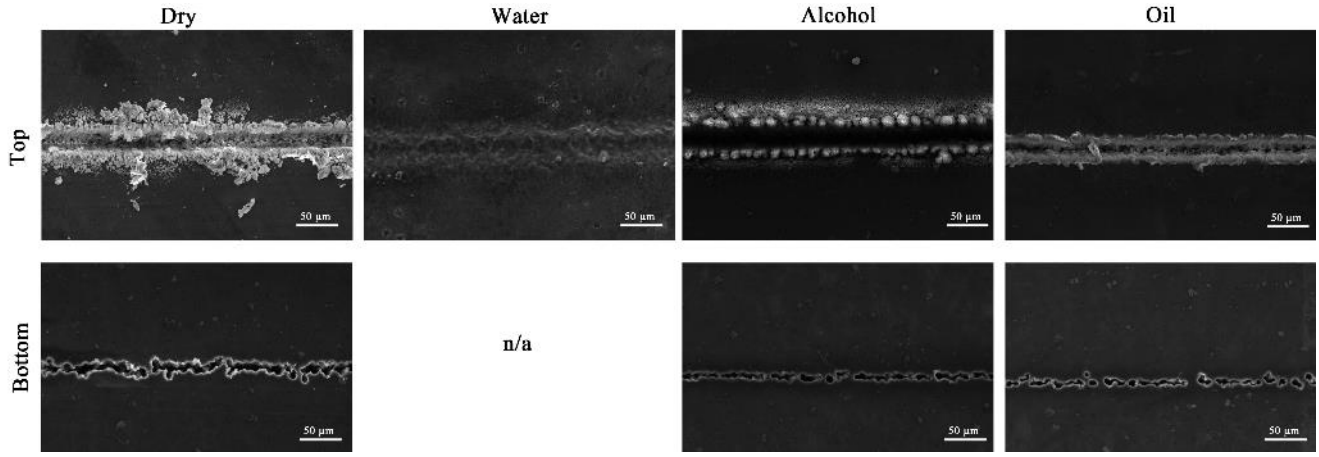

Figure 9. Comparison of dry cutting and submerged cutting conditions with 0.5 mm liquid height and 2.75 mm cutting speed.

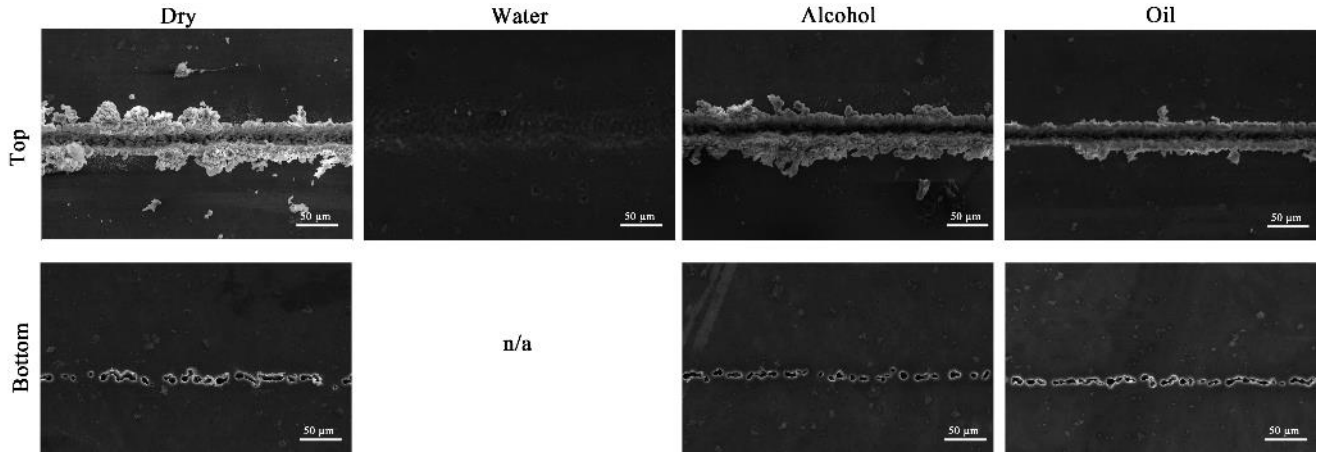

Figure 10. Comparison of dry cutting and submerged cutting conditions with 0.5 mm liquid height and 5.25 mm cutting speed.

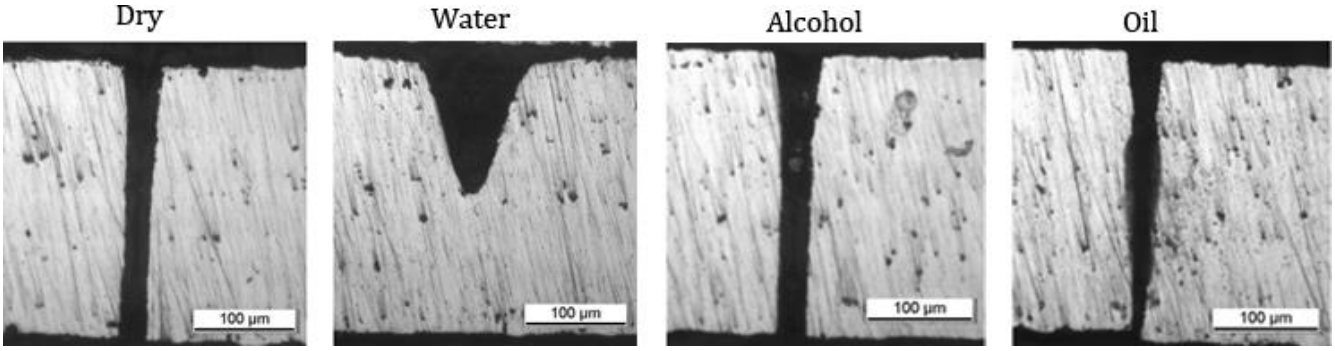

Figure 11. Cross section of dry cutting and submerged cutting conditions with 0.5 mm liquid height and 0.25 mm cutting speed.

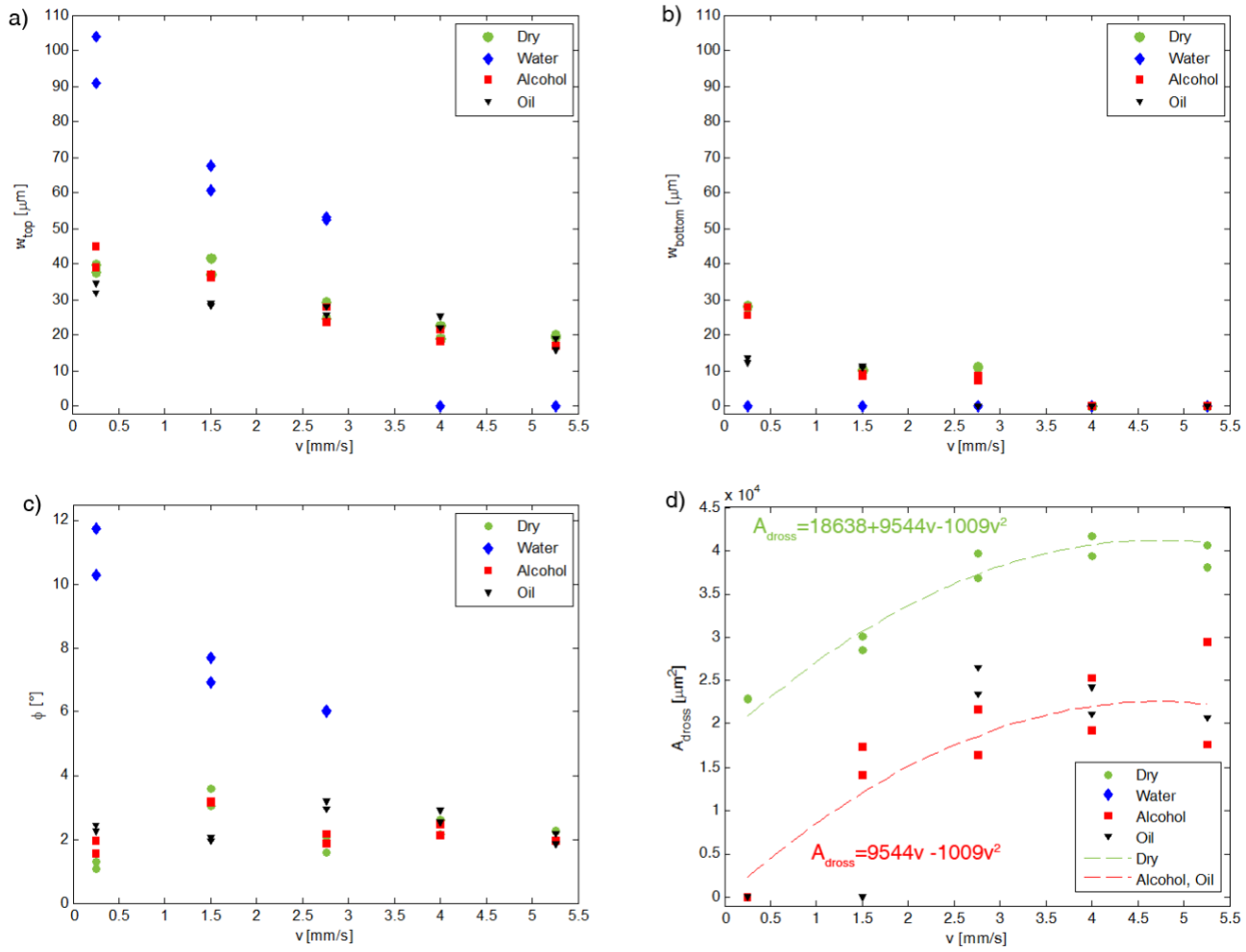

Figure 12. a) Top and b) bottom kerf width, c) resultant taper angles, d) dross area as a function of cutting liquid and speed (h_l=0.5 mm).

The analyses on the geometrical characteristics give insights to the physical phenomenon. It can be observed that an alcohol film on the material surface does not change the cutting conditions significantly compared to dry operation. The limited liquid height does not attenuate or enlarge the beam significantly, contributes to material dissolution with chemical attack and does not alter the beam path by mechanical effects due to high volatility. Oil behaves much similar to alcohol, providing a dross-free surface. However, its higher viscosity renders the material ejection from the bottom side of the kerf more difficult, accumulating dross inside the kerf. The cut quality is reduced in water due to liquid breakdown. It can be concluded that the optimal condition consists of submerging in 0.5 mm alcohol-water solution with cutting speed at 0.25 mm/s.

4.2. Comparison with conventional laser micro-cutting and discussion

The results showed dross-free cutting is achievable once processing condition that enables chemical dissolution of dross without excessive fluence loss or liquid instability is determined. For the present Mg alloy, the optimal condition was found by submerging in 0.5 mm alcohol-water solution and cutting speed at 0.25 mm/s. In this condition, the cut quality is superior to CW and ns-pulsed cutting and comparable to that obtained with a fs laser using a conventional head with coaxial gas supply [5]. As a matter of fact, the best quality obtained on fs-laser cut AZ31 showed powderous residue of approximately 20 μm extent around the kerf and inside. Despite the high cut quality, the powder residue was required to be cleaned through a light chemical etching step. A similar cleaning step would be necessary also in the present case, however for mainly smoothing the cut edge. On the other hand, the main drawback of the submerged cutting remains as the lower productivity. The fs-pulsed and ns-pulsed systems could cut the 0.2 mm thick material with 5 mm/s and 4 mm/s speed respectively.

The results obtained in this work can be interpreted for designing new submersion liquids for cutting Mg alloys. Most of the aqueous and alcohol based solutions, without the addition of colorants, transmit well the laser wavelengths in visible and near infrared regions. The submersion liquid should be applied as a thin film ($h_l \leq 1$ mm) and should not attenuate the laser beam for more than 5%. Liquids characterized by low boiling temperature and high vapour pressure would evaporate more easily in process, avoiding liquid instabilities. High viscosity is preferable also to maintain liquid stability with workpiece motion or liquid circulation.

5. Conclusions

The present paper reports the use different liquids for submersion cutting of AZ31 Mg alloy using a low ns-pulsed green fiber laser. The main changes in the process compared conventional cutting due to the introduction of the liquid phase on the workpiece were addressed under optical, chemical and mechanical effects. An analytical solution was developed to calculate the beam fluence on the workpiece after passing through the liquid phase. The calculations depicted that the beam enlargement due to change in refractive index does not significantly reduce the fluence, however the absorptivity of the liquid can cause significant energy loss. The analysis showed that in

water and alcohol possible reactions with Mg alloy would cause material removal, whereas oil is inert. Mechanical effects were related to liquid breakdown and it was empirically observed that all liquids were susceptible to this phenomenon below the energy levels used for the cutting operation. An experimental campaign was conducted to reveal the quality of the submersion cutting as a result of the interaction of all the related phenomenon. The results show that submersion in 0.5 mm alcohol height can produce dross-free cuts, since it allows reducing negative optical and mechanical effects but induces a chemical attack on the produced dross. The optimal condition obtained in alcohol is comparable to cut quality obtained with a fs laser using a conventional head with coaxial gas supply.

The results demonstrate the feasibility of submersion approach for dross-free cutting, however some other aspects regarding the industrial applicability should be addressed. The liquid stability is a concern and it requires adequate system for maintaining the liquid height. Moreover, when thin liquid films are employed, the surface wetting plays an important role on the liquid height stability. The liquid immersion should be carried out in relatively large containers to avoid effects of meniscus formation around the edges. Circulation and filtration of the submersion liquid are also required, which are further complicated when thin liquid films are employed. The present paper also presents an approach for predicting the different effects of submersion liquids on a chosen material. The approach can be adapted to other materials for designing submersion liquids. Different solutions with also different pH levels can be also considered extending the approach to a hybrid laser/chemical machining.

Acknowledgements

The authors thank Mr. Ferdinando Fichera and Ms. Mariagrazio Franco for their support during the experimental phase. The authors also acknowledge the support from IPG Italy for their availability to use the green fibre laser system.

References

1 D. Stoeckel, C. Bonsignore, S. Duda, and M. Dunitz, “A survey of stent designs.,” Minim. Invasive Ther. Allied Technol., vol. 11, no. 4, pp. 137–47, Jul. 2002.

2 C. Momma, U. Knop, and S. Nolte, “Laser Cutting of Slotted Tube Coronary Stents – State-of-the-Art and Future Developments,” Prog. Biomed. Res., vol. 4, no. 1, pp. 39–44, 1999.

3 A. Raval, A. Choubey, C. Engineer, and D. Kothwala, “Development and assessment of 316LVM cardiovascular stents,” Mater. Sci. Eng. A, vol. 386, no. 1–2, pp. 331–343, Nov. 2004.

4 A. G. Demir, B. Previtali, and C. A. Biffi, “Fibre Laser Cutting and Chemical Etching of AZ31 for Manufacturing Biodegradable Stents,” Adv. Mater. Sci. Eng., vol. 2013, pp. 1–11, 2013.

5 A. G. Demir and B. Previtali, “Comparative study of CW, nanosecond- and femtosecond-pulsed laser microcutting of AZ31 magnesium alloy stents,” Biointerphases, vol. 9, no. 2, p. 029004, 2014.

6 A. Kruusing, “Underwater and water-assisted laser processing: Part 1 - General features, steam cleaning and shock processing,” Opt. Lasers Eng., vol. 41, no. 2, pp. 307–327, 2004.

7 A. Kruusing, “Underwater and water-assisted laser processing: Part 2 - Etching, cutting and rarely used methods,” Opt. Lasers Eng., vol. 41, no. 2, pp. 329–352, 2004.

8 A. Dupont, P. Caminat, P. Bournot, and J. P. Gauchon, “Enhancement of material ablation using 248, 308, 532, 1064 nm laser pulse with a water film on the treated surface,” J. Appl. Phys., vol. 78, no. 3, pp. 2022–2028, 1995.

9 H. W. Kang, H. Lee, and A. J. Welch, “Laser ablation in a liquid-confined environment using a nanosecond laser pulse,” J. Appl. Phys., vol. 103, no. 8, 093101 (6pp), 2008.

10 W. Charee, V. Tangwarodomnukun, and C. Dumkum, “Laser ablation of silicon in water under different flow rates,” Int. J. Adv. Manuf. Technol., vol.78, pp. 19–29, 2015.

11 L. S. Jiao, E. Y. K. Ng, L. M. Wee, and H. Y. Zheng, “The effect of assist liquid on the hole taper improvement in femtosecond laser percussion drilling,” Phys. Procedia, vol. 19, pp. 426–430, 2011.

12 C. Li, X. Shi, J. Si, T. Chen, F. Chen, S. Liang, Z. Wu, and X. Hou, “Alcohol-assisted photoetching of silicon carbide with a femtosecond laser,” Opt. Commun., vol. 282, no. 1, pp. 78–80, 2009.

13 L. Li and C. Achara, “Chemical Assisted Laser Machining for The Minimisation of Recast and Heat Affected Zone,” CIRP Ann. - Manuf. Technol., vol. 53, no. 1, pp. 175–178, 2004.

14 N. Muhammad, D. Whitehead, A. Boor, and L. Li, “Comparison of dry and wet fibre laser profile cutting of thin 316L stainless steel tubes for medical device applications,” J. Mater. Process. Technol., vol. 210, no. 15, pp. 2261–2267, 2010.

15 N. Muhammad and L. Li, “Underwater femtosecond laser micromachining of thin nitinol tubes for medical coronary stent manufacture,” Appl. Phys. A Mater. Sci. Process., vol. 107, no. 4, pp. 849–861, 2012.

16 J. J. Chang, B. E. Warner, E. P. Dragon, and M. W. Martinez, “Precision micromachining with pulsed green lasers,” J. Laser Appl., vol. 10, no. 6, p. 285, 1998.

17 M. J. Jackson and W. O’Neill, “Laser micro-drilling of tool steel using Nd:YAG lasers,” J. Mater. Process. Technol., vol. 142, no. 2, pp. 517–525, 2003.

18 M. R. H. Knowles, G. Rutterford, D. Karnakis, and a. Ferguson, “Micro-machining of metals, ceramics and polymers using nanosecond lasers,” Int. J. Adv. Manuf. Technol., vol. 33, no. 1–2, pp. 95–102, 2007.

19 L. Tunna, A. Kearns, W. O’Neill, and C. J. Sutcliffe, “Micromachining of copper using Nd:YAG laser radiation at 1064, 532, and 355 nm wavelengths,” Opt. Laser Technol., vol. 33, no. 3, pp. 135–143, 2001.

20 A. G. Demir and B. Previtali, “Remote cutting of Li-ion battery electrodes with infrared and green ns-pulsed fibre lasers,” Int. J. Adv. Manuf. Technol., vol. 75, no. 9–12, pp. 1557–1568, 2014.

21 K. Hock, B. Adelmann, and R. Hellmann, “Comparative Study of Remote Fiber Laser and Water-Jet Guided Laser Cutting of Thin Metal Sheets,” Phys. Procedia, vol. 39, pp. 225–231, 2012.

22 J. A. Porter, Y. A. Louhisalmi, J. A. Karjalainen, and S. Füger, “Cutting thin sheet metal with a water jet guided laser using various cutting distances, feed speeds and angles of incidence,” Int. J. Adv. Manuf. Technol., vol. 33, no. 9–10, pp. 961–967, 2007.

23 S. Mullick, Y. K. Madhukar, S. Roy, S. Kumar, D. K. Shukla, and A. K. Nath, “Development and parametric study of a water-jet assisted underwater laser cutting process,” Int. J. Mach. Tools Manuf., vol. 68, pp. 48–55, 2013.

24 M. A. Ordal et al. “Optical properties of Al, Fe, Ti, Ta, W, and Mo at submillimeter wavelengths”, Appl.

Opt. vol. 27, pp. 1203-1209, 1988.

25 D. Eliezer, H. Alves. “Corrosion and oxidation of magnesium alloys”. Handbook of Materials Selection, Ed. Myer Kutz, 2002, John Wiley & Sons, Inc., New York, 267–291.

26 ChemSpider, Royal Society of Chemistry, http://www.chemspider.com/Chemical-Structure.144624.html; last access on 11/11/2014

27 P.K. Kennedy, D.X. Hammer and B.A. Rockwell, “Laser-induced breakdown in aqueous media”, Prog, Quant. Electr. vol. 21, no. 3, pp. 155-248, 1997

List of tables

List of figures